The leading modes of NH extratropical tropopause variability and their connection with stratosphere-troposphere variability

Jinju Kim[1] · Kwang-Yul Kim[1] ⓘD

Abstract

The leading modes of Northern Hemisphere tropopause variability for November–April (1979/1980–2018/2019) and the associated stratosphere-troposphere variability were analyzed based on the NCEP and ERA interim reanalysis products. For this, cyclostationary empirical orthogonal function technique is employed. The first two modes feature the intraseasonal evolution of tropopause pressure anomalies over the Arctic, which respond directly to stratospheric temperature fluctuations in association with stratospheric polar vortex variations. These two modes reflect the link between stratospheric polar vortex strength and high-latitude tropospheric circulation. The first mode represents a single-phase fluctuation of the stratospheric polar vortex from winter to early spring. The second mode describes a two-phase fluctuation of the stratospheric vortex with opposite signs in winter and in spring. Tropopause pressure anomalies near the mid-latitude tropospheric jet regions exhibit significant zonal variation. In the first mode, in particular, these mid-latitude tropopause anomalies are linked to asymmetric jet variations in the Atlantic and the Pacific regions. In regard to the Northern Annular mode, distinct vertical evolution structures of the two modes are practically related to the varying evolutionary structure of extreme vortex events with relatively long persistence.

1 Introduction

Tropopause is an interface between the dynamically active troposphere and the stably stratified stratosphere (Holton 2004; Vallis 2006). Tropopause pressure and temperature are affected by competitive influences of tropospheric and stratospheric variability. In the troposphere, heating associated with moist convection in the tropics (Frierson et al. 2006; Wong and Wang 2000) and baroclinic eddies in the extratropics (Haynes et al. 2001; Held 1982) modulate tropopause variability on relatively short timescales. In the stratosphere, heating associated with planetary-scale waves, residual meridional circulation, and stratospheric

polar vortex account for tropopause variability (Cai and Ren 2007; Highwood et al. 2000; Rieckh et al. 2014; Wang et al. 2016; Wong and Wang 2000; Zängl and Hoinka 2001; Zängl 2002). For synoptic- and monthly-scale variability in the extratropical region, the ascent of the tropopause is related to a cooling in the lower stratosphere, a warming in the upper troposphere. It is generally accompanied by anticyclonic vorticity near the tropopause altitude, which can be explained via the so-called potential vorticity (PV) inversion (Seidel and Randel 2006; Zängl and Wirth 2002). The opposite is true for the descent of the tropopause.

In particular, tropopause variability in the Northern Hemisphere (NH) extratropics is related to stratosphere-troposphere coupling such as in vortex strengthening or weakening events (Ambaum and Hoskins 2002; Jucker 2016; Tomassini et al. 2012). This coupled variability is generally characterized by changes in stratospheric polar vortex strength, latitude of mid-latitude tropospheric jet, and meridional gradient of surface pressure (Kidston et al. 2015). Some studies argue that tropospheric response to stratospheric vortex fluctuations depends on how strong and persistent they are in the lower stratosphere (Hitchcock

and Simpson 2014; Maycock and Hitchcock 2015; Runde et al. 2016) or near the tropopause altitude (Jucker 2016). Strong and persistent vortex variation at the lower stratosphere can affect the troposphere through tropospheric eddy flux (Kidston et al. 2015; Limpasuvan and Hartmann 2000; Simpson et al. 2009), and through the anomalous tropospheric relative vorticity induced by the tropopause height fluctuation (Ambaum and Hoskins 2002; Lorenz and Deweaver 2007; Tomassini et al. 2012). In this context, tropopause can be an important factor in understanding stratospheric vortex fluctuations and their coupling with tropospheric fluctuations.

To investigate the fundamental characteristics of tropopause variation, Barroso and Zurita-Gotor (2016) and Wong and Wang (2003) analyzed the principal component of the zonal mean tropopause variability. In both studies, change in stratospheric polar vortex plays an important role in the major modes of tropopause fluctuations. However, detailed information still lacks in regard to the spatio-temporal evolution of the major modes of tropopause variability. Regional changes in the stratospheric vortex can induce zonally asymmetric effects in the tropopause and the troposphere (Mitchell et al. 2013; Seviour et al. 2016; Thompson and Wallace 2000). Tropospheric jet responses in relation to stratospheric vortex fluctuations are often stronger in the Atlantic sector than in the Pacific sector, and this pattern is closer to the North Atlantic Oscillation (NAO) pattern than the Arctic Oscillation (AO) (Davini et al. 2014; Hitchcock and Simpson 2014). With respect to positive NAO, tropopause altitude increases near the North Pole and decreases over the Iceland (Ambaum and Hoskins 2002). In this regard, zonally averaged tropopause variation may not be sufficient to reflect these characteristics. In order to understand the connectivity of the tropopause with the stratosphere and the troposphere in detail, it is necessary to investigate both the horizontal and the temporal evolutionary patterns of tropopause variability.

The purpose of this study is to identify the leading modes of extratropical tropopause fluctuations in the NH winter season. Focusing on the spatio-temporal evolution patterns, it is investigated how tropopause anomalies evolve in association with stratospheric and tropospheric anomalies. On top of the zonal mean structures, characteristics of regional variability are also discussed particularly in the Atlantic and Pacific jet regions. Furthermore, it is examined how the vertical evolution associated with the leading modes of tropopause fluctuations are related to stratospheric vortex events.

The rest of the paper is organized as follows. Data and method used in this study are described in Sect. 2. Section 3.1 introduces the major modes of the tropopause variability and Sect. 3.2 explains the dynamical relationship of tropopause variability with stratospheric and tropospheric variability. Section 3.3 shows the evolution patterns of stratospheric and tropospheric circulation and Sect. 3.4

presents tropospheric jet variation in the Atlantic and the Pacific regions. Section 3.5 deals with how the major modes of tropopause variability contribute to the vortex strengthening and weakening events in terms of polar cap averaged geopotential height variations.

2 Data and methods

2.1 Data

Winter-spring variability of tropopause pressure is extracted from 5-day mean data of the 40-year (1979–2019) NCEP daily reanalysis data. The tropopause definition used in this study is based on the lapse-rate criterion (WMO 1957). Each year represents the 36-pentad data from November 1 through April 29. To analyze the vertical linkage with key variables, the pressure-level ERA interim daily reanalysis data (Dee et al. 2011) at a $1.5° \times 1.5°$ resolution at the 37 vertical levels (1000–1 hPa) are used for the same period (1979–2018). Pressure-level variables include air temperature, geopotential height, zonal wind, meridional wind, and omega velocity. Pressure at 2 potential vorticity unit (PVU) level from the ERA interim data is also used to validate the leading modes from the NCEP tropopause pressure. The analysis domain is [0°–360° E, 30°–87.5° N].

2.2 Cyclostationary EOF analysis and regression analysis in CSEOF space

To identify the leading modes of tropopaue pressure variability, cyclostationary empirical orthogonal function (CSEOF) technique is used in this study (Kim et al. 1996; Kim and North 1997). Space–time data are decomposed into mutually orthogonal CSEOF loading vector (CSLV), $B_n(r, t)$, and mutually uncorrelated principal component time series (PCT), $T_n(t)$:

$$T(r, t) = \sum_n B_n(r, t)T_n(t), \quad B_n(r, t) = B_n(r, t + d). \quad (1)$$

In this study CSLV for each mode includes temporally varying spatial patterns with the nested period $d = 36$ pentads, which describes a physical evolution in the data. Analysis is performed on anomalies after removing the composite seasonal cycle. Area weighting is not applied since the results are not sensitive to it.

A regression analysis in CSEOF space (Kim et al. 2015) is conducted to explore stratospheric and tropospheric evolution associated with the tropopause leading modes. The regression analysis in CSEOF space is conducted as follows:

$$\text{Step 1:} \quad P(r,t) = \sum_n C_n(r,t) P_n(t), \tag{2}$$

$$\text{Step 2:} \quad T_n(t) = \sum_{m=1}^{M} \alpha_m^{(n)} P_m(t) + \varepsilon^{(n)}(t), \tag{3}$$

$$\text{Step 3:} \quad C_n^{(\text{reg})}(r,t) = \sum_{m=1}^{M} \alpha_m^{(n)} C_m(r,t), \tag{4}$$

where $T_n(t)$ is the nth PCT of tropopause pressure (target variable), $C_m(r,t)$ and $P_m(t)$ are the mth CSLV and PCT of other (predictor) variables, $\alpha_m^{(n)}$ are the regression coefficients, $\varepsilon^{(n)}(t)$ is regression error time series, M is the number of PCT used for multivariate regression ($=25$ in the present study), and $C_n^{(\text{reg})}(r,t)$ is the regressed CSLV of $P(r,t)$ associated with the nth CSEOF mode of tropopause pressure (target).

CSEOF analysis is conducted on the pressure-level key variables one level at a time (step 1), the regression is conducted on the PCT of tropopause pressure (step 2), and the regressed loading vectors of predictor variables are obtained from step 3. After the regression analysis, entire data collection can be expressed in the form:

$$\text{Data}(r,t) = \sum_n \left\{ B_n(r,t), P_n^{(\text{reg})}(r,t), U_n^{(\text{reg})}(r,t), V_n^{(\text{reg})}(r,t), \dots \right\} T_n(t), \tag{5}$$

where the spatio-temporal evolution patterns in curly braces represent loading vector of the target variable and the regressed loading vectors of predictor variables. They are all governed by the PCT of tropopause pressure, $T_n(t)$, and are physically consistent with each other. In this way, 4-dimensional (x, y, z, t) structure of variability is extracted from datasets for each mode, but time-mean or space-mean evolution patterns are displayed typically for the sake of brevity.

3 Results

3.1 Leading modes of the NH tropopause pressure variation

The first two leading modes of tropopause pressure variability in the Northern Hemisphere cold season are characterized by high-latitude signals evolving on sub-seasonal time scales (Figs. 1, 2 see also Fig. S9). The two modes can also be identified from other variables such as tropopause temperature from the NCEP reanalysis and 2-PVU pressure from the ERA5 reanalysis. The first mode accounts for 12% of the total variance. This mode exhibits a persistent tropopause depression from winter to early spring; strong positive

pressure anomalies are seen in the polar region from January to March (Fig. 1a–f). The Arctic anomalies develop in an approximately concentric fashion around the North Pole. Weak positive anomalies are developed over the Atlantic sector during January–February and weak negative anomalies over the Pacific sector during February–April.

The second mode explains about 8% of the total variance. The second mode indicates a winter-spring oscillation of the Arctic tropopause anomalies, which consists of a relatively weak winter signal and a relatively strong spring signal of opposite signs (Fig. 2). Negative anomalies exist in the polar region in December–February with a phase transition in February leading to positive anomalies in March–April (Fig. 2a–f). In addition to the development of these Arctic-centered anomalies, local anomalies also develop across the hemisphere. They are particularly apparent in November, December, and February when the Arctic signal is not so strong or is in the stage of phase transition.

The PC time series corresponding to each mode shows a large interannual variation in both modes (Figs. 1g and 2g). Lagged correlation between the two PC time series is generally insignificant within the range of ± 72 pentads ($-0.19 < r < 0.04$) (figure not shown); this suggests that the two leading modes are statistically independent and derive from different physical processes. The PC time series of the first mode is weakly correlated with interannual variation of the Arctic Oscillation (AO) (-0.41 with the ± 17-pentad smoothed AO index). This paper investigates the spatio-temporal evolution of several key physical variables corresponding to the positive phase of the PC time series in order to understand the physical mechanisms associated with the first two CSEOF modes of tropopause pressure. For the negative phase, the results are the same except for the opposite signs.

Results in this section show that the two leading CSEOF modes of tropopause pressure variability are characterized by zonally asymmetric signals dominant in the Arctic. The first mode represents a strong increase in tropopause pressure in the Arctic, lasting from January to March. The second mode shows a relatively weak reduction of tropopause pressure in December–February and a relatively strong increase in March–April.

3.2 Evolution in the Arctic stratosphere and troposphere and its linkage to the Arctic tropopause variability from a zonal mean perspective

Based on the lapse-rate definition, tropopause pressure (height) is closely related to changes in the vertical gradient of temperature in the upper troposphere and lower stratosphere (UTLS) (Fig. S1a (shading) and b), i.e. changes in static stability such as the square of buoyancy frequency (Seidel and Randel 2006; Wang et al. 2016). In the Arctic
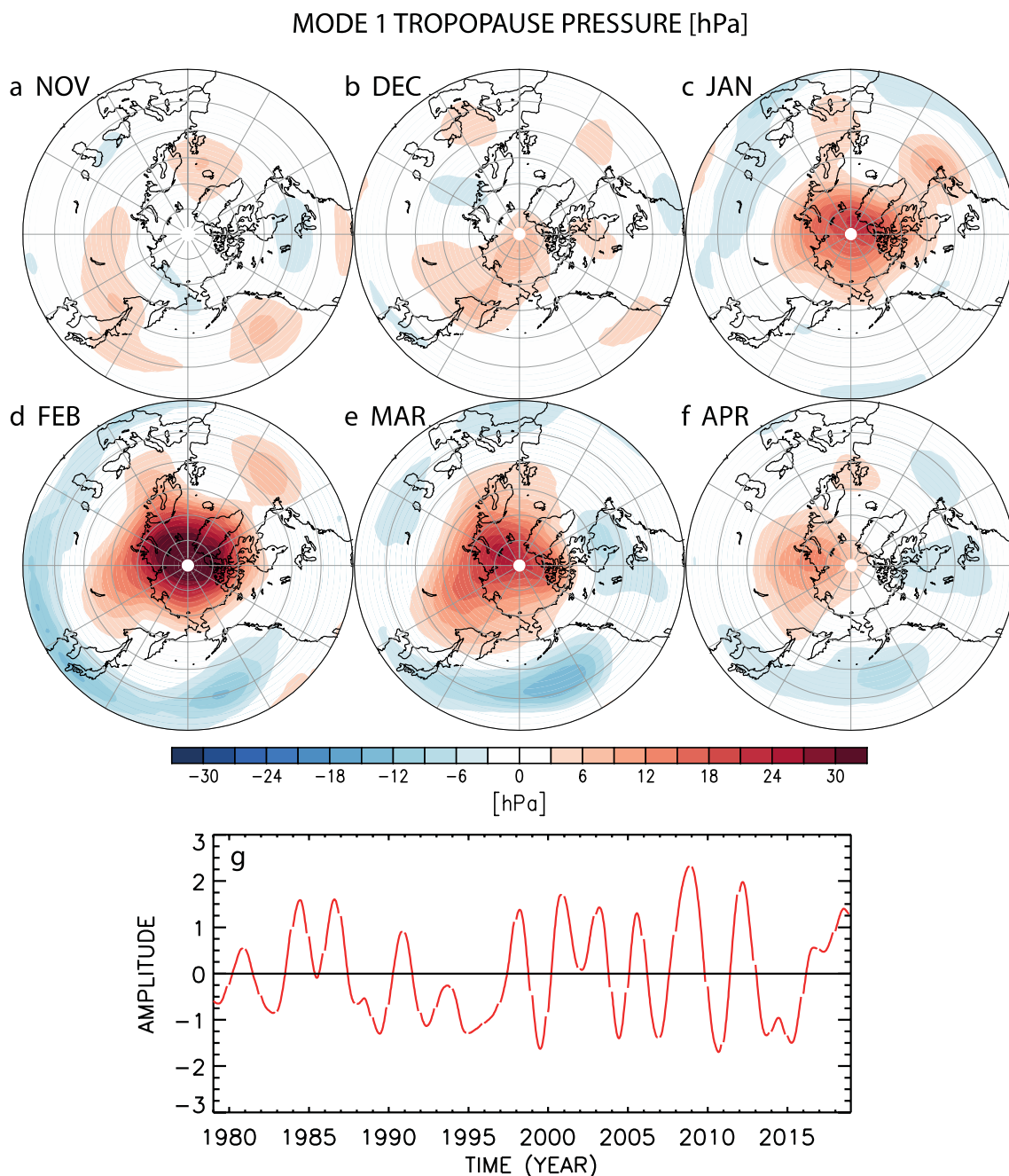
MODE 1 TROPOPAUSE PRESSURE [hPa]

Fig. 1 **a–f** Monthly mean loading vectors for the first CSEOF mode of tropopause pressure variability (hPa) and **g** the corresponding principal component time series

region, tropopause anomalies are dominantly affected by stratospheric temperature anomalies and are more closely related to stratospheric zonal wind anomalies than to tropospheric anomalies (Fig. S1a and b). Thus, a rise in Arctic tropopause pressure is largely due to an increase in the stratospheric temperature and the UTLS static stability, and is accompanied by a weakening of stratospheric westerlies that satisfy the thermal wind balance (Fig. 3). Conversely, a reduction in tropopause pressure is accompanied

by a decrease in stratospheric temperature and UTLS static stability, and a strengthening of stratospheric westerlies. This relationship is similar to the results in other studies (Ambaum and Hoskins 2002; Barroso and Zurita-Gotor 2016; Tomassini et al. 2012; Jucker 2016; Wong and Wang 2003; Zängl and Hoinka 2001).

In the first mode, temperature begins to increase in the polar stratosphere from early December, and then tropopause pressure begins to rise near the end of December.
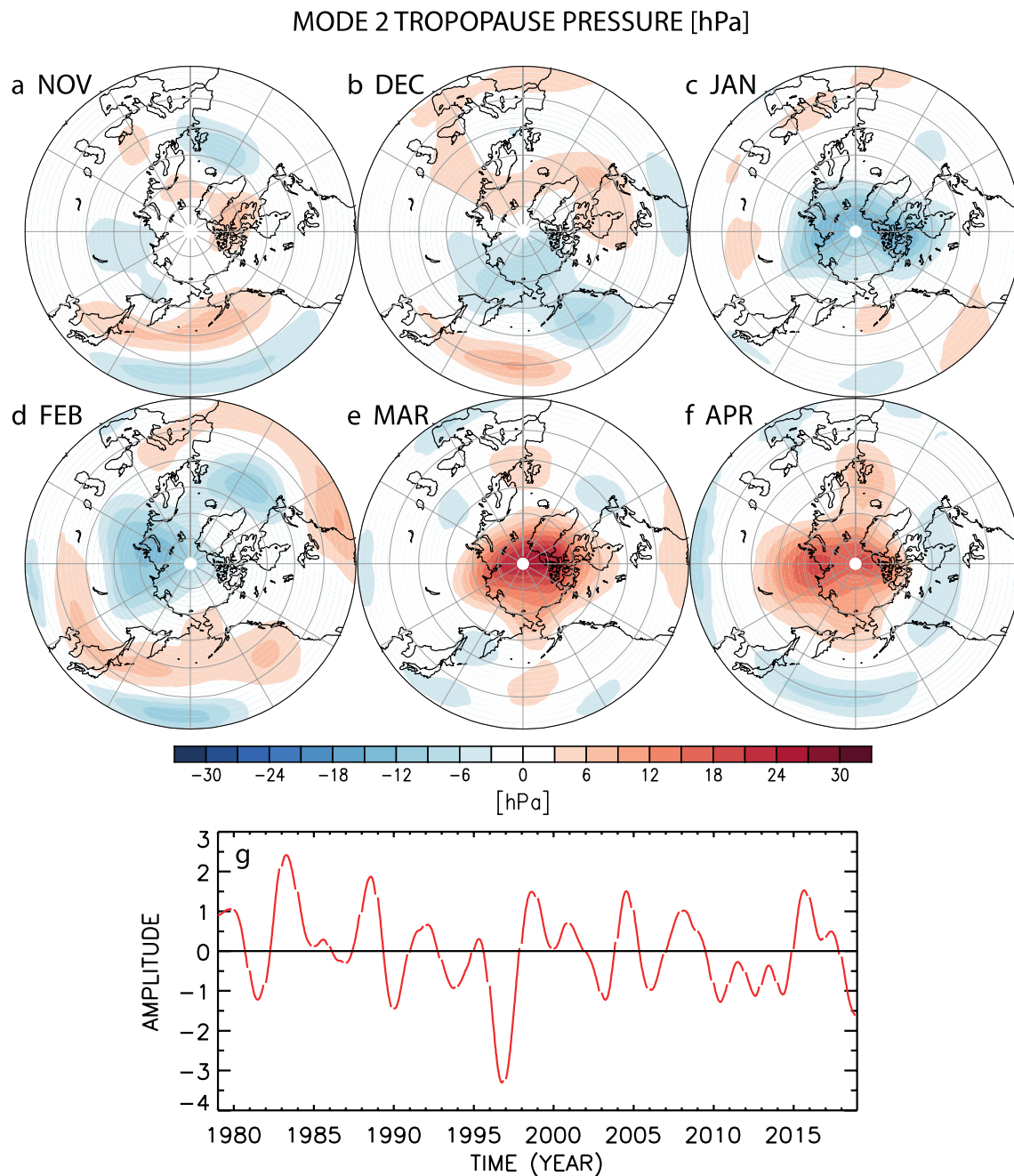
MODE 2 TROPOPAUSE PRESSURE [hPa]

Fig. 2 a–f Monthly mean loading vectors for the second CSEOF mode of tropopause pressure variability (hPa) and **g** the corresponding principal component time series

Strong temperature anomalies (see e.g., 1.5 °C contour line) gradually grow and descend for about two months (Fig. 3a). The signal peaks in mid-February and persists until early April in the lower stratosphere. This increase in temperature indicates a weakening of the cold stratospheric polar vortex. In association with the positive temperature anomalies, negative static stability anomalies develop above them and positive static stability anomalies develop near the tropopause (shading in Fig. 3b). It seems that the stratospheric warming and a subsequent increase in static stability near the tropopause result in a rise in tropopause pressure (shading in Fig. 3a, b). The positive static stability anomalies near the tropopause also explain positive PV anomalies there (contours in Fig. 3b). Change in PV near the tropopause is dominated by the static stability component than the absolute vorticity component (figure not shown). Anomalous tropospheric cooling develops from February (Fig. 3a). This tropospheric cooling can
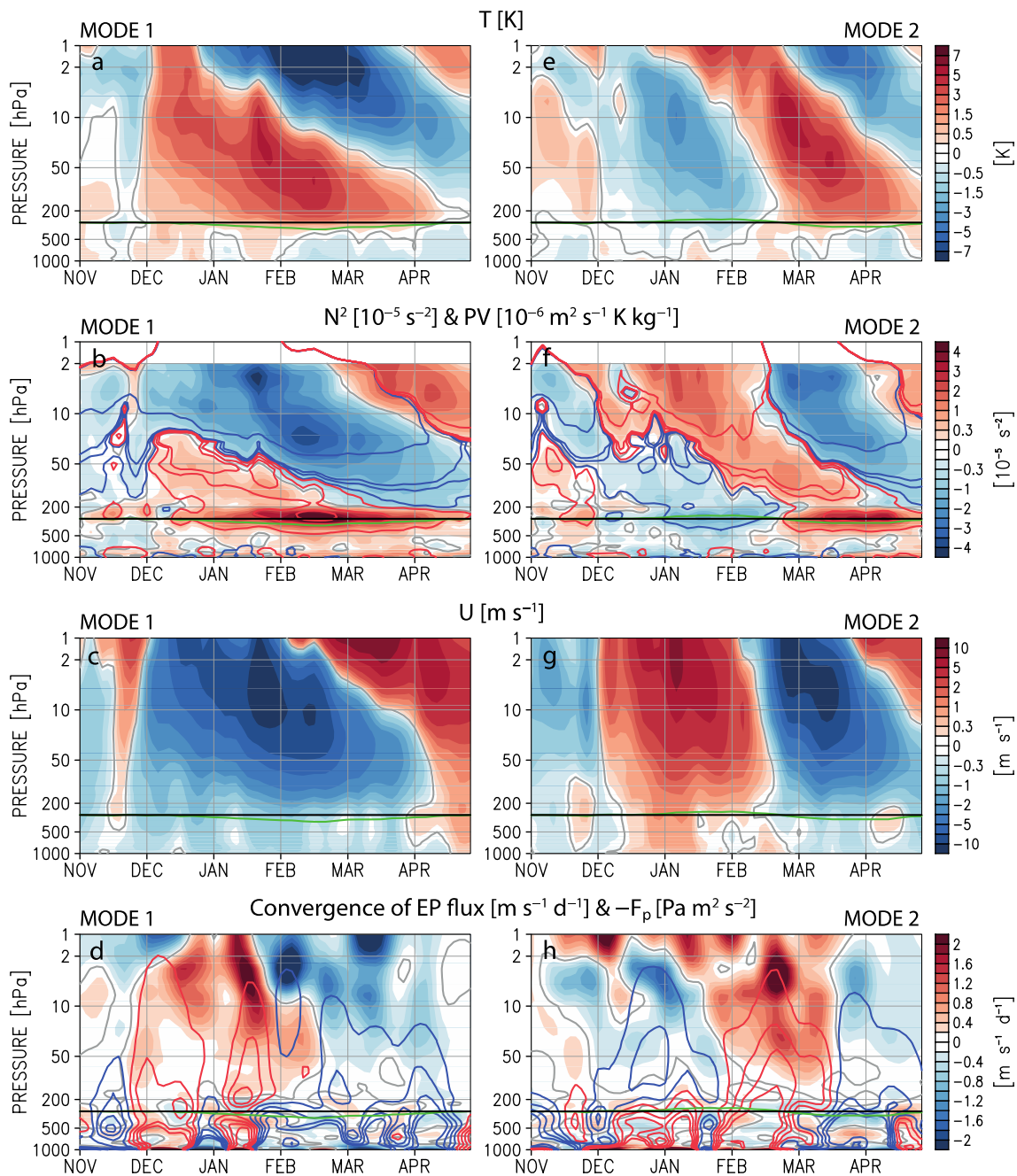
Fig. 3 Time-altitude zonal mean patterns of **a**. **e** 65°–87° N averaged air temperature anomalies (K), **b**, **f** 65°–87° N averaged static stability anomalies (shading, 10^{-5} s^{-2}) and potential vorticity anomalies [red (+) and blue (−) contours at ± 0.05, 0.3, 0.5, and 5 PVU (10^{-6} m^2 s^{-1} K kg^{-1})], **c**, **g** 50°–80° N averaged zonal wind anomalies (m s^{-1}), and **d**, **h** 50°–80°N averaged convergence of EP flux anomalies (shading, m s^{-1} day^{-1}) and vertical EP flux anomalies [red (upward) and blue (downward) contours at ± 0.5, 1.5, 2.5, and 3.5×10^5 Pa m^2 s^{-2}] and tropopause fluctuations (green line) for the **a–d** first and **e–h** the second CSEOF modes of tropopause variability. The tropopause fluctuation is obtained by adding a 3σ value of the anomalous field to the climatology. The grey line depicts the zero contour of the shaded anomalies

further intensify the tropopause pressure increase induced by stratospheric warming.

The development of the positive temperature anomalies is linked thermodynamically with that of negative zonal wind anomalies (Fig. 3c). This change in zonal mean zonal wind

is attributable to the variation of the Eliassen-Palm (EP) flux divergence (shading in Fig. 3d) (Baldwin and Dunkerton 2001; Polvani and Waugh 2004; Thomson and Wallace 2000), which is dominated by the vertical component of EP flux anomalies (contours in Fig. 3d). Similar to the

positive temperature anomalies, negative zonal wind anomalies develop in the upper stratosphere from early December (Fig. 3c). This is related to prominent upward EP flux anomalies throughout the troposphere and stratosphere and their convergence in the stratosphere during late November–mid-February (Fig. 3d). The bottom level of the anomalous convergence seems to descend toward the tropopause, which is consistent with the downward expansion of the zonal mean stratospheric easterly (Limpasuvan et al. 2004, 2005) (Fig. 3d and Fig. S2). In February–April, downward flux and divergence of EP flux anomalies are dominant in the stratosphere. They are related to a reduction in the anomalous easterly wind and a subsequent phase transition to the anomalous westerlies in the stratosphere.

In the second mode, negative temperature anomalies first appear from the upper stratosphere in early December and change to positive anomalies during February (Fig. 3e). The UTLS static stability and tropopause pressure display negative anomalies from the end of December and positive anomalies from the end of February (shading in Fig. 3f). PV anomalies near the tropopause also show evolution similar to the tropopause pressure anomalies (contours in Fig. 3f). The spring phase with a peak in March is relatively strong compared to the winter phase with a peak in January. The evolution of the second mode exhibits a shorter duration of about 2 months and a half and a faster growth and a shorter descending time scale of about 1 month for each phase compared to the first mode (Fig. 3a, e). The second mode describes a strengthening of the cold stratospheric polar vortex in winter and a weakening in spring.

Together with the negative and positive temperature anomalies, positive and negative zonal wind anomalies appear in the stratosphere (Fig. 3g). The evolution of the vertical EP flux anomalies and divergence with alternating signs in the stratosphere coincide with the variation of zonal mean flow (Fig. 3h). The direction of the vertical EP flux anomalies in the stratosphere is opposite to that in the troposphere during December–January, but the direction thereafter is the same throughout the stratosphere and troposphere (contours in Fig. 3h). The detailed latitude-altitude structures of several zonal mean variables are briefly discussed in the supplementary information (Fig. S3 and S4).

In both modes, the anomalous zonal mean flow started from the upper stratosphere is clearly traced in the troposphere; evolution coherent in phase appears in the troposphere (contours in Fig. 4a, d and Fig. S5). In connecting the zonal mean flow in the stratosphere and that in the troposphere, variation of eddy momentum flux seems to play an important role (Limpasuvan et al. 2004; Simpson et al. 2009). This momentum flux is negatively proportional to the meridional component of EP flux. In the first mode, when anomalous easterlies occupy the lower stratosphere, northward EP flux is dominant in the upper troposphere

(shading in Fig. 4a, d). The northward EP flux corresponds to southward eddy momentum flux, which decelerates the zonal mean flow in higher latitudes and accelerates the zonal mean flow in lower latitudes (second column in Fig. S2). This anomalous eddy momentum forcing is consistent with easterly wind anomalies in the polar region. Along with these momentum flux anomalies, Eulerian mean meridional circulation develops, which consists of anomalous northward wind in the upper troposphere, anomalous southward wind in the lower troposphere (shading in Fig. 4b) and anomalous downward motion in the Arctic region (contours in Fig. 4b). Coriolis force acting on the meridional wind anomalies induces westerly momentum in the upper troposphere and easterly momentum in the lower troposphere (shading in Fig. 4b). In the perspective of momentum balance, the westerly wind anomaly driven by Coriolis force in the upper troposphere attenuates the easterly wind anomaly driven by divergence of momentum flux anomaly (shading in Fig. 4a, b). On the other hand, in the lower troposphere, the easterly wind anomaly driven by Coriolis force is partially offset by surface friction. Therefore, eddy momentum forcing as well as related mean meridional circulation play a crucial role in the evolution of tropospheric zonal wind anomaly with the same polarity as the high-latitude stratospheric zonal wind anomaly (Limpasuvan et al. 2004; Simpson et al. 2009). These relationships can also be seen in the second mode (Fig. 4d, f). When anomalous westerly prevails in the lower stratosphere during winter, southward EP flux anomalies are dominant in the upper troposphere (shading in Fig. 4d). They are accompanied by anomalous southward winds in the upper troposphere, anomalous northward winds in the lower troposphere (shading in Fig. 4e), and anomalous upward motion in the Arctic region (contours in Fig. 4e). As anomalous easterly develops in the stratosphere in spring, anomalous meridional EP flux and associated anomalous mean meridional circulation are reversed.

The zonal-mean zonal wind variations in the subpolar region coincide with the polar cap averaged geopotential height (PCH) variations in the lower troposphere (bars in Fig. 4c, f). PCH anomalies show more complicated fluctuations than the tropopause anomalies (black line in Fig. 4c, f), which are directly affected by the low-frequency change in the lower stratospheric temperature. In the first mode, while the tropopause pressure increases, PCH increases along with easterly anomalies in the troposphere (Fig. 4a, c). The northward EP flux anomalies peak at the end of January, and become relatively weak in February early March. However, the intensity of the positive height anomalies tends to be maintained during this period. This may be partly related to the tropospheric column compression effect due to the tropopause height decrease: a reduction in the height of the tropospheric column as a result of stratospheric warming reduces relative vorticity below, which is associated with an increase
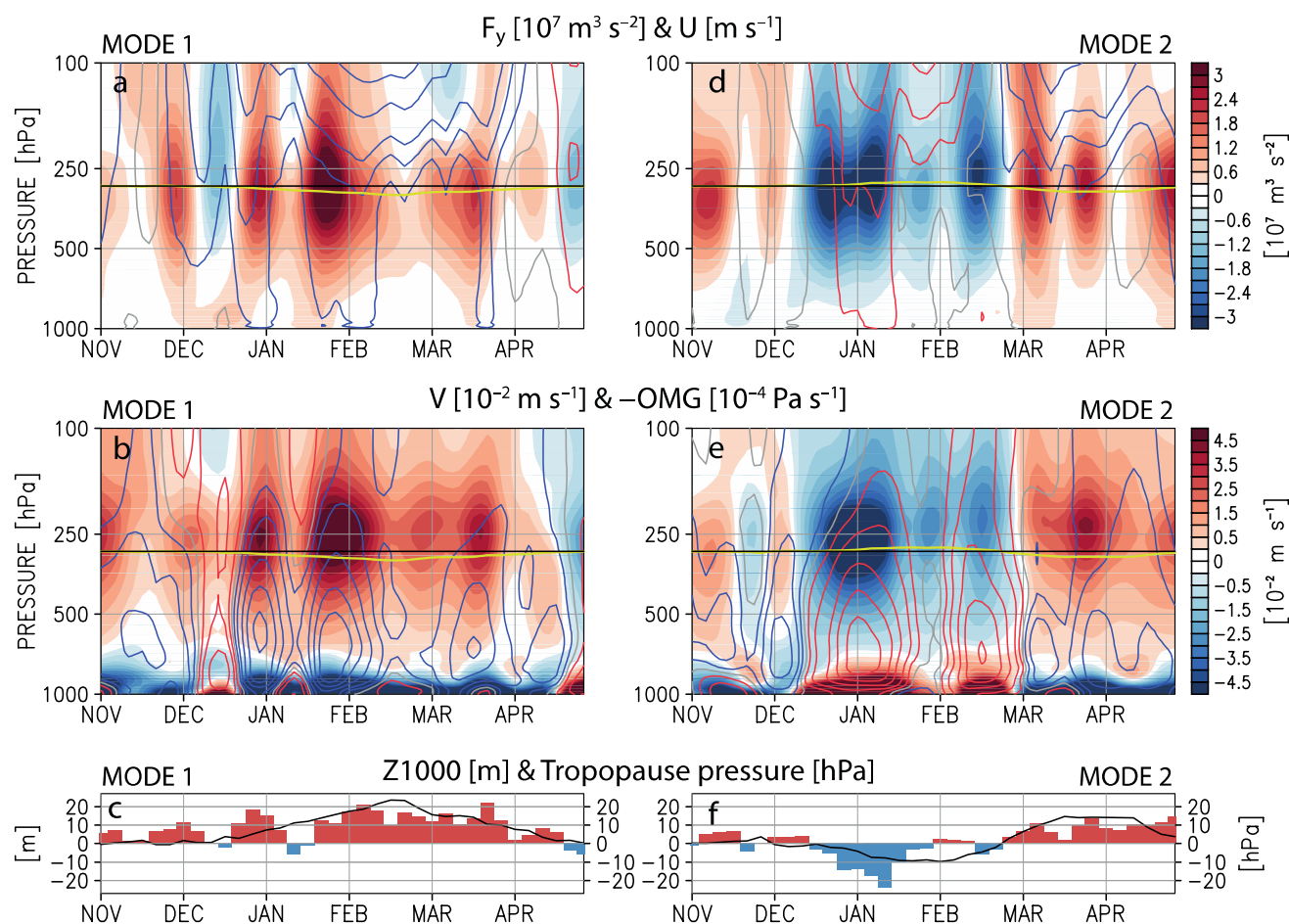
Fig. 4 Time-altitude zonal mean patterns of **a**, **d** 40°–70° N averaged meridional EP flux anomalies (shading, 10^7 m^3 s^{-2}) and 50°–80° N averaged zonal wind anomalies [red (+) and blue (−) contours at ±0.5, 1.5, 2.5, and 3.5 m s^{-1}], **b**, **e** 40°–70° N averaged meridional wind anomalies (shading, 10^{-2} m s^{-1}) and 65°–87° N averaged vertical (−ω) wind anomalies [red (upward) and blue (downward) contours at ±2, 5, 10, 15, and 20×10^{-4} Pa s^{-1}], tropopause fluctuations

(yellow line), **c**, **f** 65°–87°N averaged geopotential height anomalies (color bar, m) at 1000 hPa and tropopause pressure anomalies (black line, hPa) for the **a–c** first and **d–f** the second CSEOF modes of tropopause variability. The tropopause fluctuation is obtained by adding the climatology with the 1σ values of the anomalous field. The grey line depicts the zero contour of the contoured anomalies

in surface pressure (Ambaum and Hoskins 2002; Tomassini et al. 2012) (Fig. S5). The relationship between the stratospheric polar easterly anomaly and the positive anomalies in the tropopause pressure and near-surface geopotential height can also be explained in terms of global mass circulation (Cai and Ren 2007; Kidston et al. 2015). Convergence of EP flux anomalies associated with the stratospheric polar easterly anomaly induces a strengthening of the residual meridional circulation (third column in Fig. S2). As a result, anomalous air inflow and descending motion above the polar region increase tropopause pressure and surface pressure.

In the second mode, like the tropopause pressure fluctuation, tropospheric PCH exhibits negative winter anomalies followed by positive spring anomalies (bars in Fig. 4f). However, tropopause and tropospheric PCH anomalies evolve differently in the detail (black line in Fig. 4f). In

the winter phase, negative anomalies of PCH develop and decline more rapidly than the anomalous tropopause pressure. On the other hand, positive anomalies of PCH last longer than the anomalous tropopause pressure in the spring phase.

The main point of this section is that the two modes of tropopause pressure are strongly linked to changes in stratospheric polar vortex strength and are coupled with coherent evolution throughout the stratosphere and troposphere in the Arctic. In other higher modes, tropopause anomalies are less correlated with upper-middle stratospheric variations (Fig. S6), and surface pressure anomalies evolve differently from the anomalies related to stratospheric and tropopause fluctuations (Fig. S5). That is, the downward effect of the upper stratospheric vortex fluctuations tends to be relatively weak in other higher modes. This means that

stratosphere-troposphere coupled variability with vertically coherent evolution is tied with the two tropopoause modes.

3.3 Horizontal evolution patterns of the stratospheric and tropospheric circulation

Figures 5 and 6 depict monthly averaged horizontal evolution of geopotential height and zonal wind anomalies. In the first mode, positive height anomaly develops in the Arctic stratosphere but is slightly shifted to the northern Europe in February, like a climatological stratospheric vortex (shading in Fig. 5c). Easterly wind anomaly surrounding the positive height anomaly reduces stratospheric polar jet speed in all sectors. That is, these stratospheric anomalies depict that the stratospheric polar vortex weakens and its center migrates toward the northern Europe, particularly during December–February (green dashed contour in Fig. 5a–c). The polar high and easterly anomalies last until March in the lower stratosphere (Fig. 5f–j). In February–March, the polar easterly and mid-latitude westerly winds are shifted further south in the North Atlantic and further north in the North Pacific (contours in Fig. 5h, i).

In the lower troposphere, anomalous high is observed in the Barents Sea-Ural region during December, which is favorable to enhance upward EP flux of zonal wavenumber 1 and 2 (shading in Fig. 5k). With the stratospheric vortex weakening, positive height anomaly appears over Iceland and the Arctic in January (Fig. 5l). The Arctic high anomaly is strong until March and the surrounding easterly wind anomaly stays strong in the Atlantic region (shading in Fig. 5l–n). Low anomalies seen to the south of the Arctic high anomaly reminds the negative AO/NAO circulation patterns. In the Pacific sector, however, low anomaly is located at higher latitudes than in a typical AO condition during February and March, and positive height anomaly is dominant in mid-latitudes (shading in Fig. 5m, n). This is similar to the tropospheric pattern over the Pacific region during late winter–spring in association with the weakening of stratospheric polar vortex in Zhang et al. (2019). The polar easterly and mid-latitude westerly winds in the Pacific, located further north than in the Atlantic as in the lower stratosphere, are related to these zonally asymmetric height anomalies in mid-latitudes. In addition to a weak correlation between the PC time series and the AO index, the circulation patterns indicate that the first mode contributes, at least partially, to the interannual variation of the AO (or NAO when zonal asymmetry is considered) in January–March (see also Fig. S7).

The winter phase of the second mode shows negative height anomaly in the upper stratosphere, which is centered near the Chukchi Sea (shading in Fig. 6a, b). Westerly wind anomaly surrounding the negative height anomaly is relatively weak over Eurasia. Nevertheless, when anomalies are fully developed during January, the climatological stratospheric polar jet accelerates in all sectors (contours in Fig. 6b). These polar westerly anomaly and polar low anomaly also appear in the lower stratosphere and the troposphere (Fig. 6g, l). In the lower troposphere, positive height anomalies in the Atlantic and northeastern Pacific surrounding the low anomaly is reminiscent of a positive phase of the AO (shading in Fig. 6l).

During December, height anomalies with opposite signs alternate from the northwestern Pacific to Greenland in the lower stratosphere (shading in Fig. 6f). This pattern is similar to the pattern of anomalous tropopause pressure anomalies in December (Fig. 2b). In particular, negative height anomaly over Greenland becomes stronger from mid-December, and poleward momentum flux develops strongly in the North Atlantic region (figure not shown). This momentum flux, which is related to strong equatorward EP flux anomalies in late December–early January (shading in Fig. 4d), may be linked to a reduction in upward EP flux toward the stratospheric polar vortex (Figs. 3h and S3).

From mid-February, positive height anomaly and easterly wind anomaly begin to develop in the Arctic stratosphere (Figs. 3g, 6c–e). The anomalous easterly is related to an increase in upward EP flux associated with the tropospheric high anomalies in the North Atlantic and Ural region and the tropospheric low anomaly in the northwestern Pacific during the phase transition period (shading in Fig. 6m). In the lower stratosphere and troposphere, positive height anomaly develops over the Arctic from March and continues through April (shading in Fig. 6i, j, n, o). In the lower troposphere, mid-latitude low anomalies are seen over Europe and the central North Pacific. The meridional gradient of height anomalies is opposite to that in the winter phase (shading in Fig. 6l, n). Compared with the tropospheric pattern in January, the center of action of the mid-latitude height anomalies is shifted slightly eastward (westward) in the Atlantic (Pacific) sector and the polar height anomalies are more asymmetric in the zonal direction.

The perturbed vortex in the second mode shows a development in which its center moves toward the pole as the vortex strengthens in December–January (green dashed contour in Fig. 6a, b), and then moves to the northern Europe as it weakens in March (Fig. 6d). The strong stratospheric anomalies in March can exert a strong influence on the fragile spring vortex, much greater than the impact of winter anomalies on the strong winter vortex (Fig. 6b, d).

This section shows that the center of stratospheric vortex shifts toward the northern Europe as it weakens and its center moves closer to the pole as it strengthens. This is true for both the modes even though the evolution patterns are different. In the lower troposphere, AO/NAO-like pattern appears in both modes. Mid-latitude anomalies, however,

Fig. 5 Monthly mean patterns of **a–e** 10-hPa geopotential height anomalies [shading, m] and 10-hPa zonal wind anomalies [red (+) and blue (−) contours at ±3, 6, 9, and 12 m s^{-1}] with the seasonal cycle of climatological geopotential height (green solid contour at 30,170 m) and perturbed geopotential height (green dashed contour at 30,170 m), **f–j** 150-hPa geopotential height anomalies [shading, m] and 150-hPa zonal wind anomalies [red (+) and blue (−) contours at ±0.5, 1.5, 2.5, and 3.5 m s^{-1}], and **k–o** 1000-hPa geopotential height anomalies (shading, m) and 700-hPa zonal wind anomalies [red (+) and blue (−) contours at ±0.5, 1, 1.5, and 2 m s^{-1}] for the first CSEOF mode. The perturbed geopotential height is obtained by adding the climatology with the 1σ values of the anomalous geopotential height. 30,170 m contour is considered as a polar vortex boundary, which corresponds to geopotential height contour at climatological zonal wind maximum location
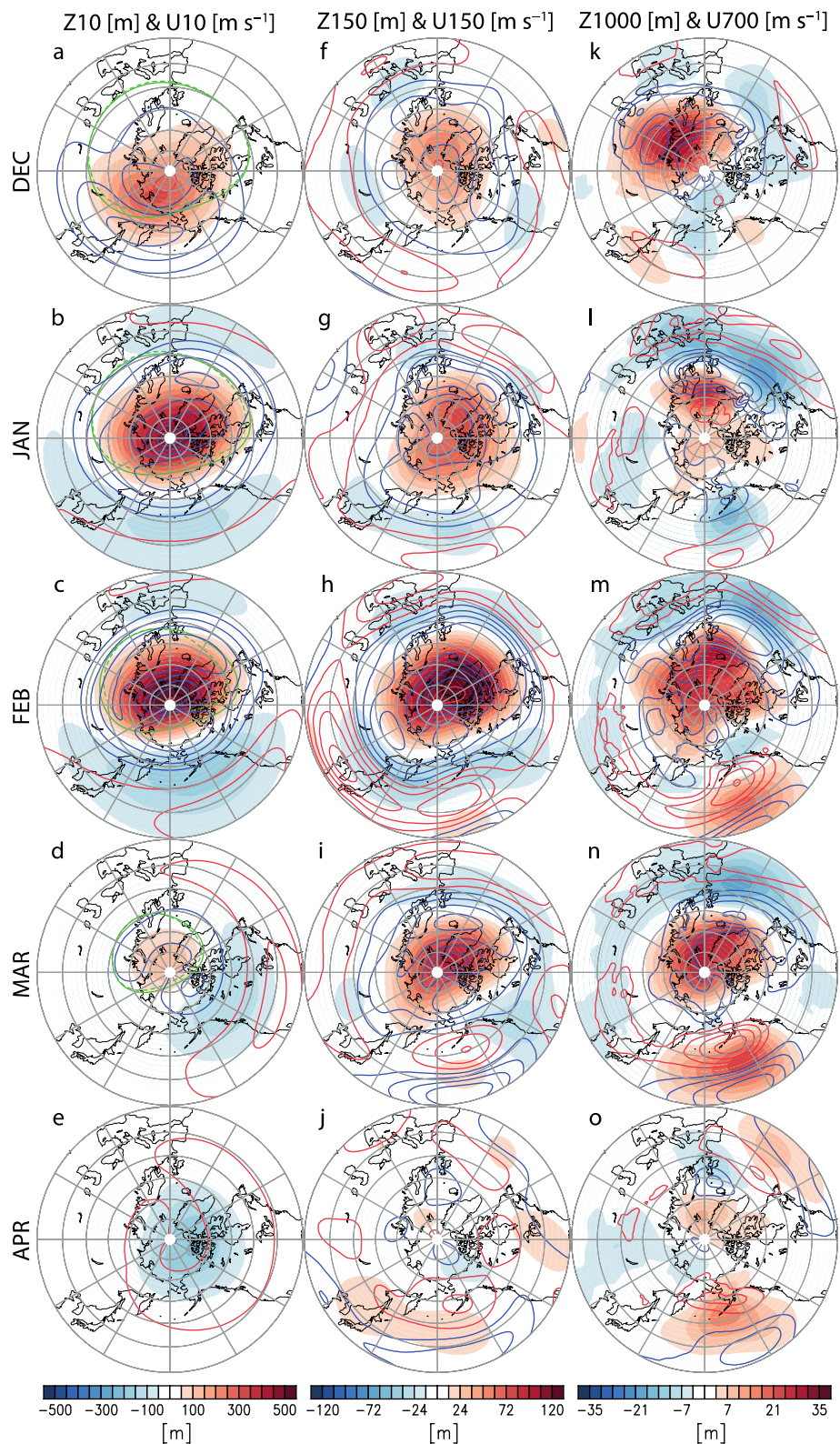

exhibit significant zonal asymmetry and do not evolve in the same manner as the high-latitude anomalies. These regional variations will be discussed further in the next sections in terms of tropospheric jet fluctuations in the Atlantic and Pacific regions.

Fig. 6 Monthly mean patterns of **a–e** 10-hPa geopotential height anomalies [shading, m] and 10-hPa zonal wind anomalies [red (+) and blue (–) contours at ± 3, 6, 9, and 12 m s^{-1}] with the seasonal cycle of climatological geopotential height (green solid contour at 30,170 m) and perturbed geopotential height (green dashed contour at 30,170 m), **f–j** 150-hPa geopotential height anomalies [shading, m] and 150-hPa zonal wind anomalies [red (+) and blue (–) contours at ± 0.5, 1.5, 2.5, and 3.5 m s^{-1}], and **k–o** 1000-hPa geopotential height anomalies [shading, m] and 700-hPa zonal wind anomalies [red (+) and blue (–) contours at ± 0.5, 1, 1.5, and 2 m s^{-1}] for the second CSEOF mode. The perturbed geopotential height is obtained by adding the climatology with the 1σ values of the anomalous geopotential height. 30,170 m contour is considered as a polar vortex boundary, which corresponds to geopotential height contour at climatological zonal wind maximum location
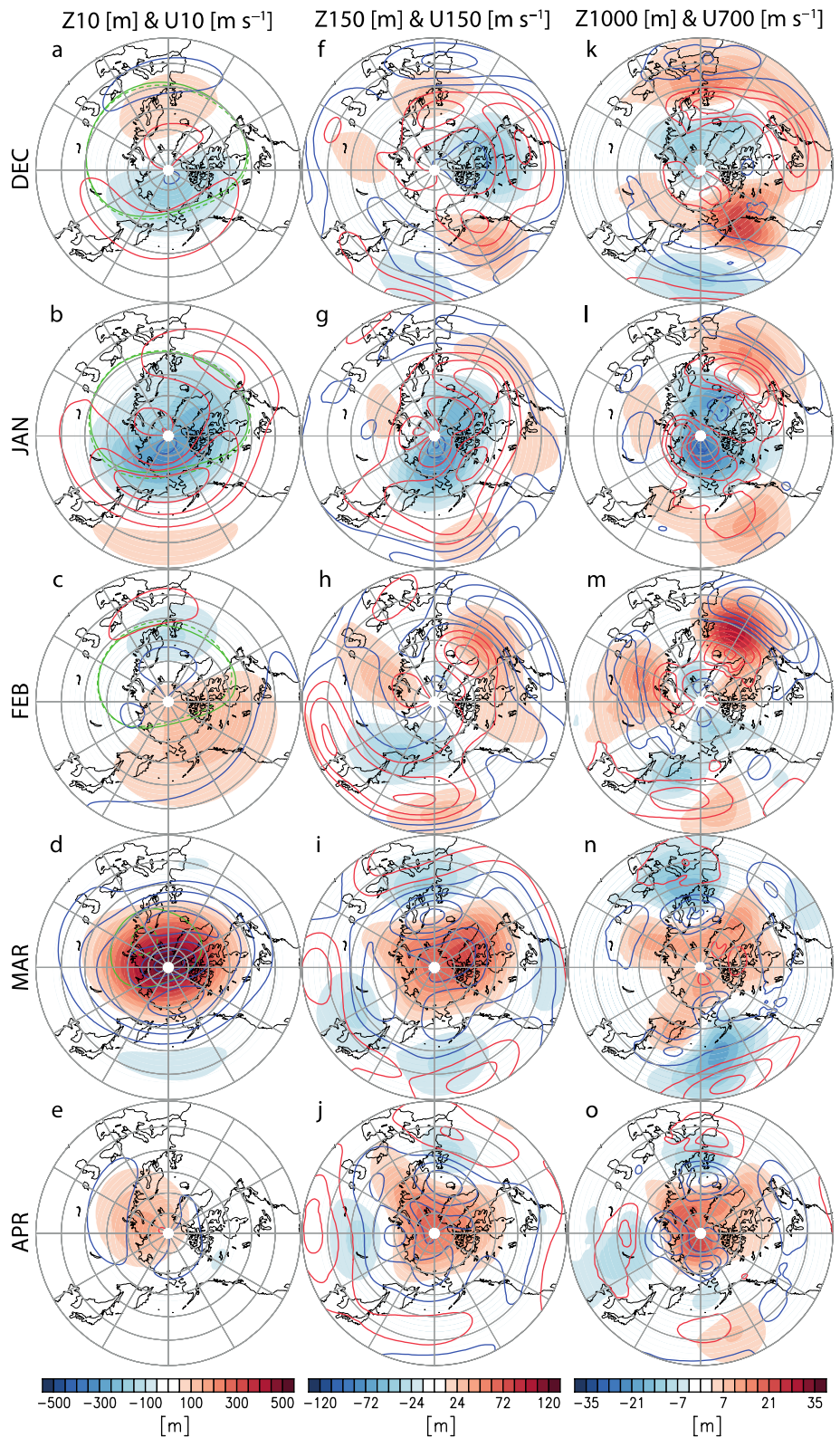
3.4 Mid-latitude tropospheric jet fluctuation and its linkage to the tropopause undulation

The temporally varying centers of action in mid-latitude circulation anomalies cause regional differences in the response of the tropospheric jets. Tropospheric jets behave differently in the Atlantic and Pacific regions, indicating regionally asymmetric stratosphere-troposphere coupling. This is clearly seen in the first mode (Fig. 7a–f). The easterly anomaly decelerates the poleward side and the mid-latitude westerly anomaly accelerates the equatorward side of the Atlantic jet (shading in Fig. 7a–c). The Atlantic jet axis moves equatorward, which is frequently accompanied by the weakening of stratospheric polar vortex (Kidston et al. 2015). The polar easterly anomaly is located further

north in the Pacific region and barely affects the Pacific jet (Fig. 7d–f). The weakened impact of stratospheric polar jet deceleration on the Pacific jet is due to the large meridional separation, and is similar to the result of Davini et al. (2014). In January, the tropospheric Pacific jet is strengthened by the mid-latitude westerly anomaly (Fig. 7d). In February and March, the axis of the Pacific jet migrates poleward (triangle symbols in Fig. 7e, f), which is the opposite to the jet movement in the Atlantic (Fig. 7b, c).

The mid-latitude tropopause anomalies are much weaker and smaller, which nonetheless reflect the tropospheric jet variations. The anomalous tropopause pressure gradient is, in general, positively correlated with the tropospheric zonal wind variation near the jet stream (Fig. S8). This, from the PV perspective, is because positive (negative) tropopause
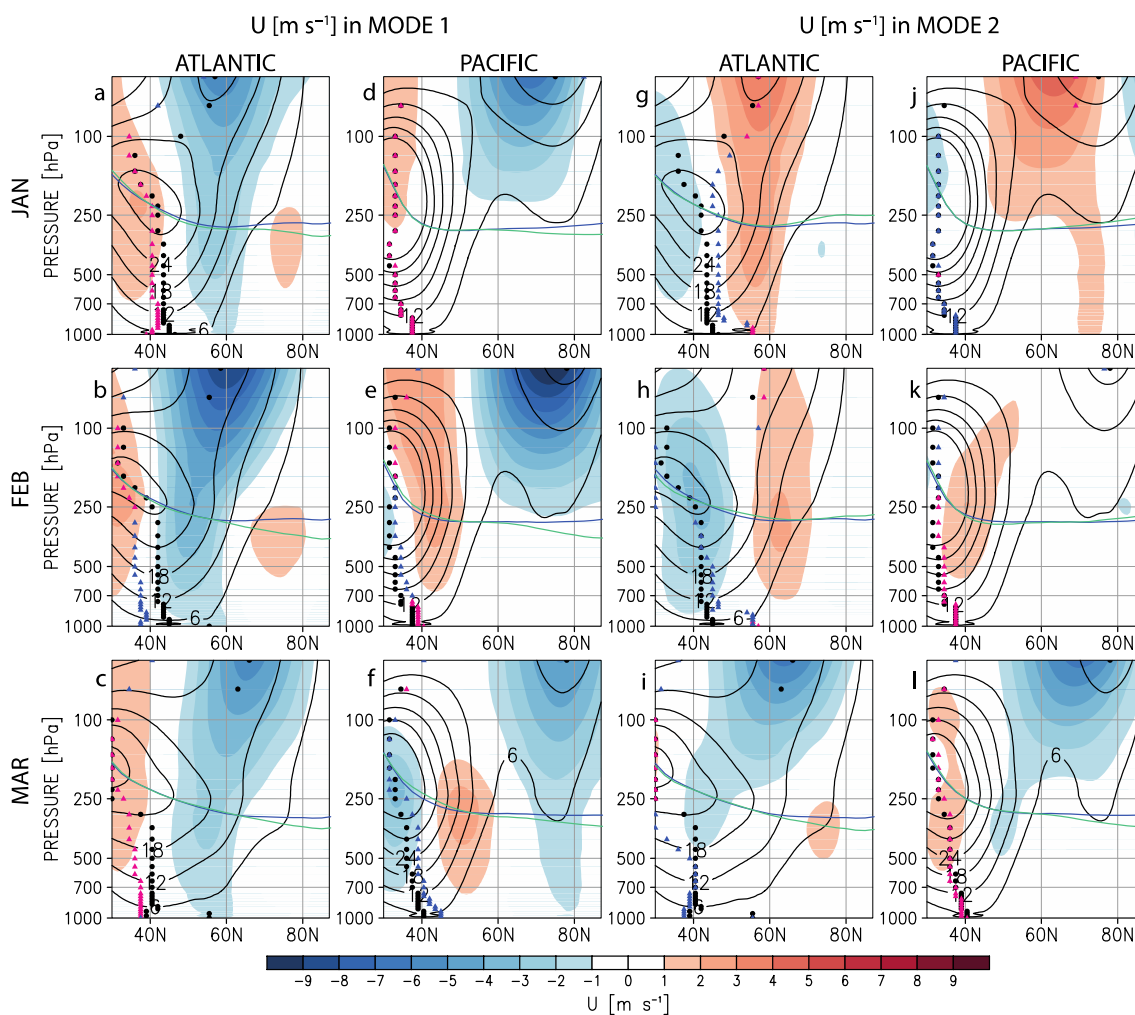

Fig. 7 Latitude-altitude monthly mean patterns of zonal wind anomalies [m s^{-1}] (shading) and climatological zonal wind [contours at 6 m s^{-1} interval] and jet axis of the climatology (black circle) and perturbed wind (color triangle, red: acceleration, blue: deceleration) and the climatological tropopause (blue line) and perturbed tropo-

pause (aqua line) over **a–c**, **g–i** the Atlantic [90°–10° W] and **d–f**, **j–l** the Pacific [120°–230° E] regions during the period of strong stratospheric variation in **a–f** the first and **g–l** the second CSEOF mode of tropopause variability. The perturbed field is obtained by adding the climatology with the 2σ values of the anomalous field

pressure anomalies are dynamically balanced with cyclonic (anticyclonic) anomalies at the UTLS region (Seidel and Randel 2006; Zängl and Wirth 2002). In this regard, the tropospheric cyclonic anomaly in the Atlantic region coexists with the positive tropopause pressure anomaly in the first mode (Figs. 1c–e, 7a–c). In the Pacific region, the tropospheric anticyclonic anomaly coexists with the negative tropopause pressure anomaly (Figs. 1c–e, 7d–f).

This relationship is relatively clear in the mid-latitude tropopause, which contrasts with the high latitude tropopause where strong coupling with stratospheric vortex fluctuations results in decorrelation with tropospheric height variations (Figs. S1a and b and S6f). It can be said, therefore, that the mid-latitude tropopause anomalies are more closely linked to tropospheric wind anomalies than the Arctic tropopause anomalies. This relationship with the tropospheric jet also appears in the zonal mean sense, which explains the wavy deformation of tropopause anomalies to the north and south of the zonal wind anomalies through meridional flux of quasigeostrophic PV at the tropopause level (Barroso and Zurita-Gotor 2016).

Unlike the first mode, where the latitude of the stratospheric polar jet anomaly differs in the Pacific and Atlantic sectors, both polar jet anomalies develop around 60° N in the second mode (shading in Fig. 7g–l). In January, intensification of the stratospheric polar vortex is manifested as an acceleration on the polar side of the Atlantic and Pacific jets (Fig. 7g, j). The Atlantic jet migrates poleward, but the Pacific jet shows no latitudinal shift in its axis and slows down slightly. In February, when the stratospheric vortex fluctuation begins to weaken, a poleward migration of the Atlantic jet, along with deceleration, is seen in the mid-lower troposphere (Fig. 7h). At this time, the Pacific jet speeds up (Fig. 7k). Weakening of the stratospheric vortex in March is connected with the weakening of the Atlantic jet strength and deceleration on the polar side of the Pacific jet (Fig. 7i, l). In addition, the Pacific jet is strengthened as opposed to January. The associated mid-latitude tropopause anomalies and their gradient are more complicated than the first mode, particularly in the Pacific (Fig. 2c, e and Fig. S8).

In summary, tropospheric jet fluctuations not only are different in the two oceanic sectors but also vary in time despite the persistence of the stratospheric vortex fluctuation in the first mode. In the second mode, it is found that the change in the mid-latitude jets is not simply of opposite signs in January and March as in the stratospheric vortex. From a regional perspective, these results indicate that zonal asymmetry in the variation of stratospheric and tropospheric zonal winds is an important characteristic of the leading modes of tropopause variability.

3.5 Role of the two modes in the extreme stratospheric vortex events

Reconstructed data based on the two modes accounts for more than 40 (50) % of the total variance of the PCH index at 10 (50) hPa. In addition, the reconstructed data are significantly correlated with the raw data in the stratosphere with a correlation value of ~ 0.65 (~ 0.74) at 10 (50) hPa (Fig. 8 and Fig. S10). As can be seen in Fig. 8, evolution patterns of the PCH anomalies are reasonably similar between the two, although significant differences are also seen in some years. This suggests that PCH variability in the stratosphere can be explained to some extent in terms of the two CSEOF modes. More precisely, the PCH variability can be explained to some extent by the stratospheric fluctuations that induce the Arctic tropopause fluctuations in the two modes. In the troposphere, however, the PCH variability associated with the leading modes of tropopause pressure tend to be obscured because of strong internal variability (Fig. S10). In this study, the normalized PCH index is used as a proxy for the Northern Annular Mode (NAM) index, which describes variation of the polar vortex strength (Baldwin and Dunkerton 2001; Baldwin and Thompson 2009). If a local extremum of the 10-hPa NAM index is greater than $+1.5\sigma$, a weak vortex event is assumed to have occurred, and a strong vortex event is assumed to have occurred if it is less than -1.5σ. Thresholds are generally set to ± 1–3σ (Baldwin and Dunkerton 2001; Limpasuvan et al. 2004, 2005), and in this study, the same threshold as in Runde et al. (2016) is used. The minimum distance between two adjacent events is set to 12 pentads (2 months) based on the peak date of each event; any two events not separated by the minimum distance are considered as a single event and the larger of the two peaks is chosen as the strength of the extreme event. For composite analysis, the strongest event in each polarity for a given year is used.

The tropopause-related vertical evolution explains the long persistency of typical extreme vortex events (Fig. 9). The two modes contribute to the gradual decline of weak vortex (WV) events in the stratosphere (Fig. 9a–f); without the two modes a weak vortex event will in general end quickly (within a month). The two modes are also strongly responsible for the intensity and the persistence of strong vortex (SV) events in the stratosphere (Fig. 9g–l). However, it seems that contribution from other CSEOF modes is additionally needed to fully explain the asymmetry between the positive and negative events in other studies (Huang et al. 2017; Limpasuvan et al. 2005; Martineau and Son 2010).

In addition to the composite characteristics of extreme vortex events, it should also be noted that their evolution characteristics and the timing of occurrence vary significantly from one case to another. The two modes not only explain the total PCH variation to some extent as mentioned

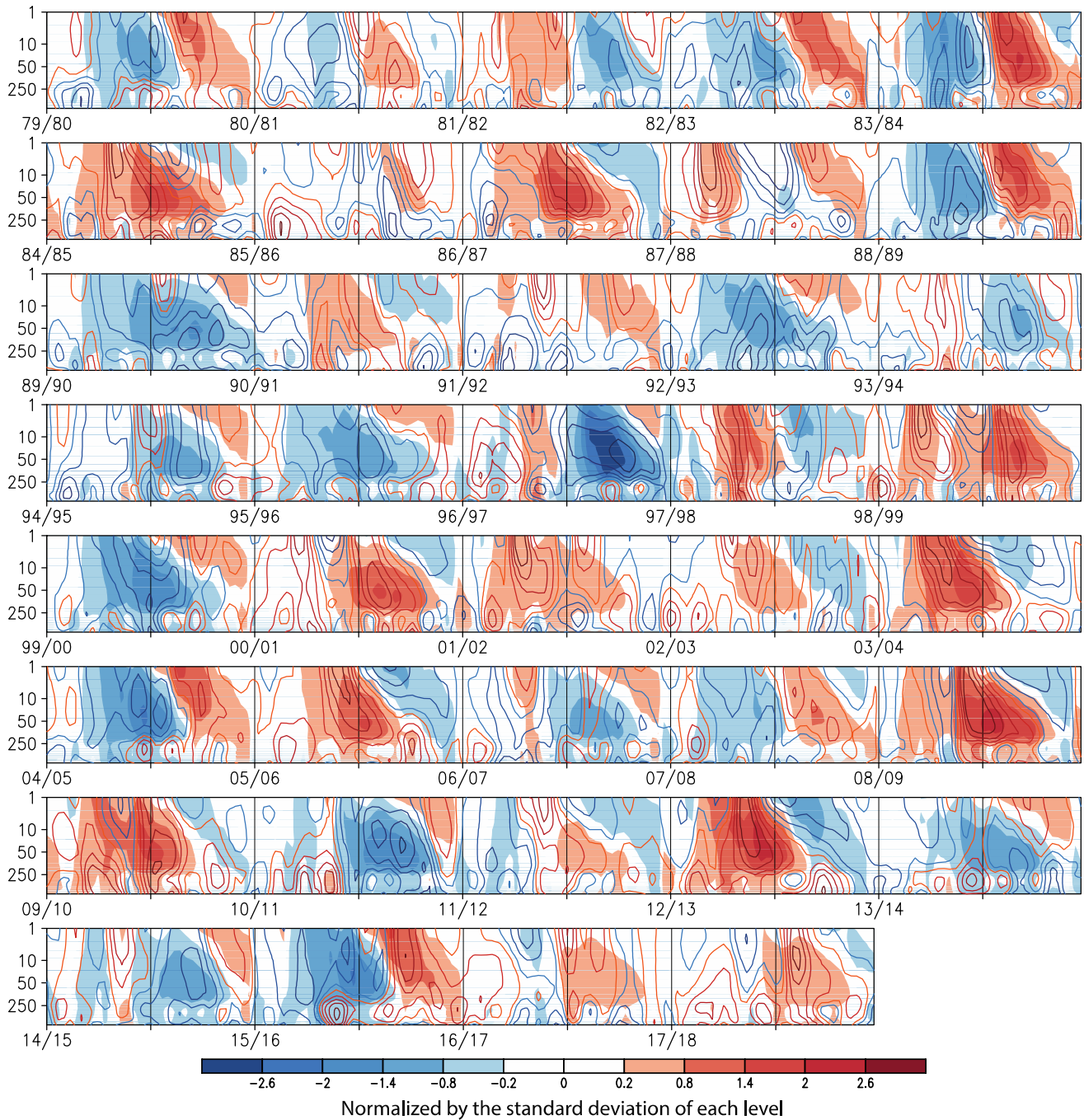### Normalized polar cap averaged geopotential height anomalies

Fig. 8 Normalized polar cap averaged [0°–360° E, 65°–87° N] geopotential height (PCH) anomalies from the reconstructed data based on the first two CSEOF modes of tropopause variability (shaded) and that from the raw data (contour) during the data period (1979–2018)

above, but also explain reasonably the intraseasonal evolution of stratospheric vortex each year. The irregular interplay of the two modes with distinctive evolutionary characteristics is expected to produce the diversity of vortex events. Therefore, it is necessary to distinguish the contributions

of the two modes in order to understand how they shape the individual characteristics of vortex events.

Figure 10 depicts the amplitudes of the first and the second modes for each vortex event, and shows fairly uneven contributions of the two modes. This figure shows only the cases when the 10-hPa PCH index of the two-mode
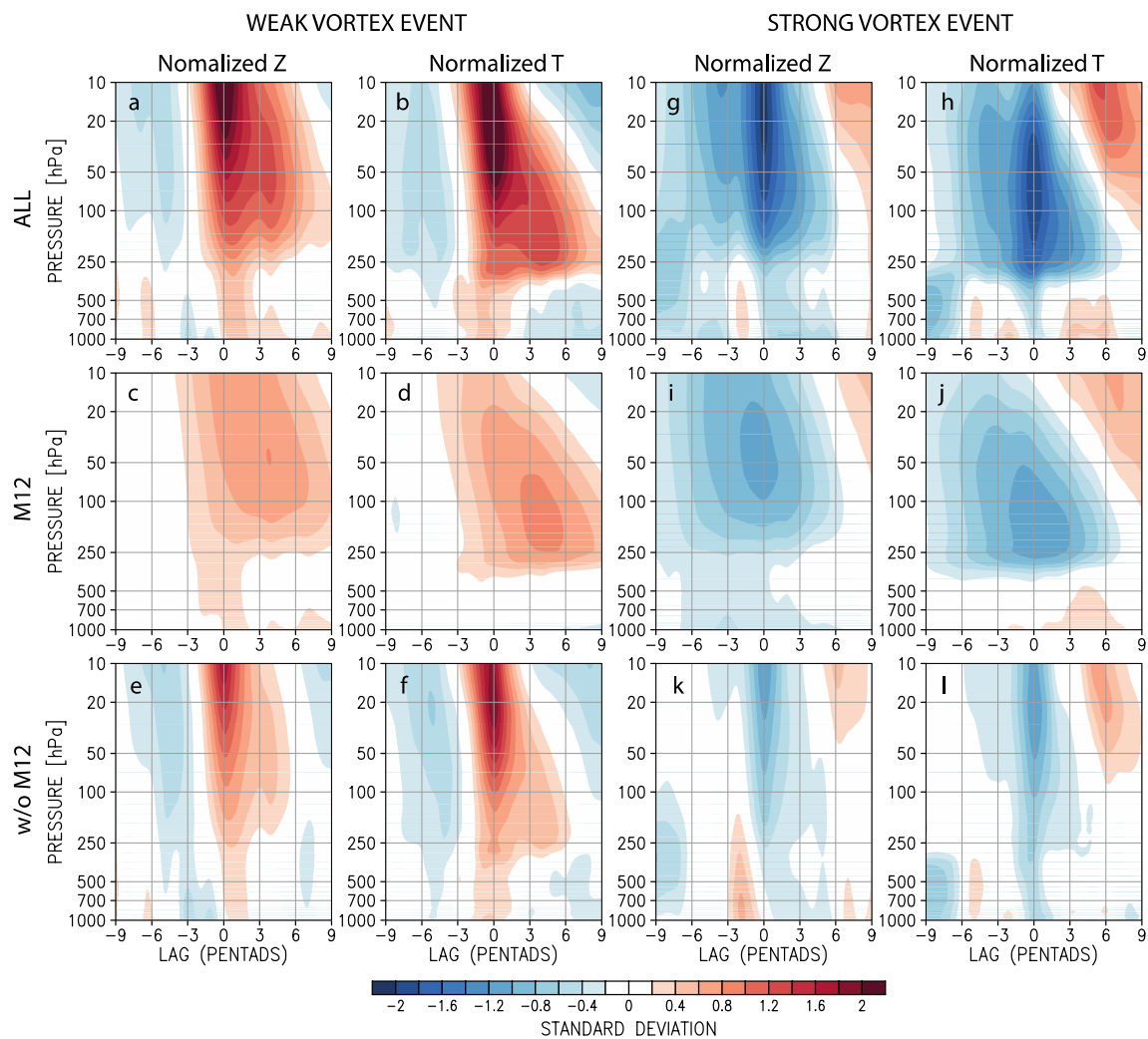
WEAK VORTEX EVENT

STRONG VORTEX EVENT

Fig. 9 Composite time-altitude patterns of the normalized polar-cap averaged [0°–360° E, 65°–87°] (the first and third columns) geopotential height anomalies and (the second and fourth columns) temperature anomalies for **a–f** the weak events and **g–l** the strong events of the stratospheric polar vortex. The first row represents the raw data, the second row is based on the first two CSEOF modes, and the third row represents the raw data without the first two CSEOF modes. The 10-hPa polar cap height (PCH) index greater (less) than $+1.5\sigma$ (-1.5σ) is defined as the weak (strong) vortex events. For composite patterns, the strongest event of each polarity in a given year is used. The abscissa denotes lag in pentads with respect to the timing of the strongest event

reconstruction has the same polarity as the event on the peak date. Since the two modes of the tropopause pressure are characterized by low-frequency modulation, their superposition is insufficient to form a rapid vortex event shorter than 2 months and more than two events a year. If the amplitude of any of the two modes is greater than $+1$ or less than -1, it is considered to make an active contribution to the occurrence of the pertaining event (color symbols in Fig. 10). There are more WV events in the positive phase and more SV events in the negative phase of the first mode (Fig. 10). This indicates that WV and SV events tend to develop preferably when the first mode is in a positive and negative phase, respectively. The phase of the second mode seems to be involved in the timing of extreme events between winter

and spring. WV events in February–March are generally associated with the positive phase of the second mode, and events in January are associated with the negative phase. SV events in January–February mostly accompany the positive phase of the second mode, and events in March–April accompany the negative phase. In the same context, if both WV and SV events occur in a given year, the sequence of events is related to the phase of the second mode. In particular, when the second mode is in a positive phase, events tend to occur in the order of winter SV and spring WV (more cross symbols in the positive phase of the second mode).

To summarize, tropopause related stratosphere-troposphere variation explains the long persistence of typical extreme vortex events. For the interannual variation of
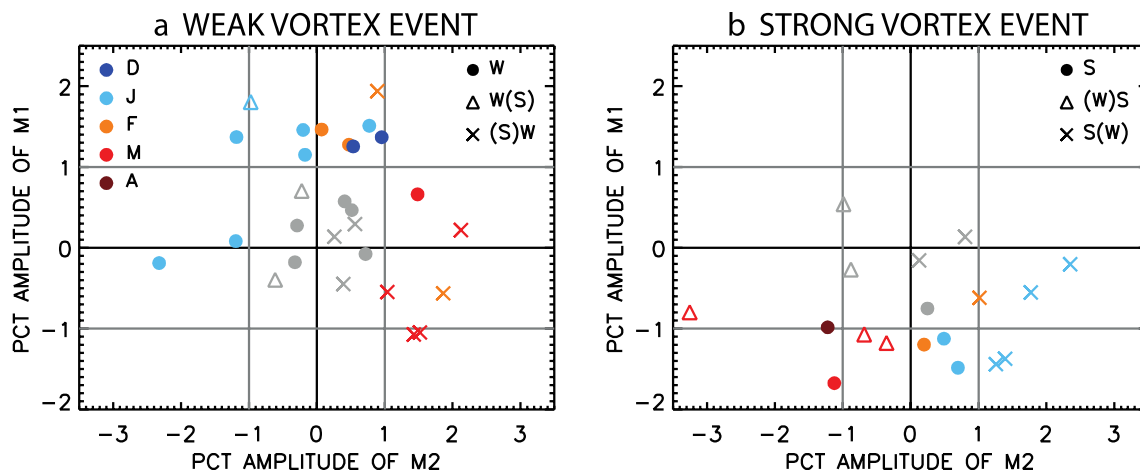
Fig. 10 PC time series amplitude of the first (*y* axis) and the second (*x* axis) modes of tropopause variability for **a** the 28 weak and **b** the 18 strong events of the stratospheric polar vortex. Events are grouped according to the following criteria: active/inactive contribution of the modes to weak/strong vortex events (color/grey symbols), occurrence of a single event in a given year (circle), and occurrence of events with both polarities in a given year (triangle: weak vortex followed by strong vortex; cross: strong vortex followed by weak vortex)

extreme vortex events, the first mode is associated with the polarity of the event, and the second mode contributes to determining the approximate timing of the event. Actual extreme vortex events occur on more diverse time scales. Nevertheless, the fact that the timing of events depends on the strength of each mode indicates that the leading two modes serve as a rough guideline for determining evolutionary structures of extreme events (Figs. 8, 10 and Fig. S10).

4 Summary and concluding remarks

In this study, the leading modes of NH tropopause pressure variability for November–April of 1979–2019 and the associated physical variation in the stratosphere and the troposphere were analyzed. The leading modes were extracted based on CSEOF analysis. The distinct evolution characteristics of the two modes in the horizontal and vertical planes and their linkage with the stratospheric and tropospheric changes were the focus of investigation. In addition, a systematic explanation for the development of extreme vortex events was attempted in terms of the two leading modes.

The first two modes, marked by anomalous tropopause pressure concentrated in the Arctic, describe connections between the stratospheric polar vortex strength and the high-latitude tropospheric circulation. Arctic tropopause pressure is directly affected by stratospheric temperature fluctuations. Stratospheric warming associated with polar vortex weakening increases Arctic tropopause pressure. The first mode reflects a stratospheric polar vortex disturbance lasting from winter to early spring. The second mode represents weak polar vortex fluctuations in winter followed by strong spring vortex fluctuations of opposite polarity.

An examination of the zonally asymmetrical component of the two modes reveals that stratospheric polar vortex weakening is linked to equatorward migration of the Atlantic jet axis and poleward migration of the Pacific jet axis in the first mode. This means that the coupling between the stratospheric polar jet and tropospheric mid-latitude jet is different in the two regions. The regional difference in the zonal wind anomalies is reflected in the mid-latitude tropopause fluctuations in terms of the PV inversion relation, which is particularly apparent in the first mode. This behavior corresponds to a tropopause pressure increase in the Atlantic and a decrease in the Pacific. For the second mode, the Atlantic jet axis moves poleward in winter, but in spring the maximum speed of the Atlantic jet only weakens without axis movement. During this period, the maximum wind speed decreases in winter and the maximum wind speed increases in spring for the Pacific jet. Compared to the first mode, however, the associated mid-latitude tropopause anomalies are much weaker and more complex.

Similar to zonal mean tropopause variability, stratospheric vortex variation plays an important role in tropopause variability (Barroso and Zurita-Gotor 2016; Wong and Wang 2003). From the spatio-temporal perspective of tropopause variation, however, mid-latitude tropopause anomalies do not develop concurrently with high-latitude anomalies and also vary in the zonal direction. Accounting for asymmetry in the zonal direction provides more detailed and realistic information about major tropopause fluctuation than a limited analysis of zonal mean variability.

It should also be noted that the two types of stratosphere-troposphere evolution can provide deeper insight into distinct evolution properties of extreme vortex events. The phase of the first mode essentially controls the polarity of

extreme events, and the phase of the second mode is strongly tied with the timing of extreme events. As a result, the super-position of physically and statistically distinct modes of tropopause variability can help understand the evolution of individual NAM events and their potential timing of occurrence, thereby improving the seasonal predictability of the Arctic climate during the cold season. This means that the leading modes of the tropopause variability can be a useful tool for understanding the slowly evolving intraseasonal interaction between the stratosphere and troposphere.

References

Ambaum MH, Hoskins BJ (2002) The NAO troposphere-stratosphere connection. J Clim 15:1969–1978

Baldwin MP, Dunkerton TJ (2001) Stratospheric harbingers of anomalous weather regimes. Science 294:581–584. https://doi.org/10.1126/science.1063315

Baldwin MP, Thompson DWJ (2009) A critical comparison of stratosphere-troposphere coupling indices. Q J R Meteorol Soc 135:1661–1672. https://doi.org/10.1175/JAS-D-15-0177.1

Barroso JA, Zurita-Gotor P (2016) Intraseasonal variability of the zonal-mean extratropical tropopause: the role of changes in polar vortex strength and upper-troposphere wave breaking. J Atmos Sci 73:1383–1399

Cai M, Ren R-C (2007) Meridional and downward propagation of atmospheric circulation anomalies. Part I: northern hemisphere cold season variability. J Atmos Sci 64:1880–1901. https://doi.org/10.1175/JAS3922.1

Davini P, Cagnazzo C, Anstey JA (2014) A blocking view of the stratosphere-troposphere coupling. J Geophys Res Atmos 119:11100–11115. https://doi.org/10.1002/2014JD021703

Dee DP, Uppala SM, Simmons AJ, Berrisford P, Poli P et al (2011) The ERA-interim reanalysis: configuration and performance of the data assimilation system. Q J Royal Meteorol Soc 137:553–597. https://doi.org/10.1002/qj.828

Frierson DMW, Held IM, Zurita-Gotor P (2006) A gray-radiation aquaplanet moist GCM. Part I: static stability and Eddy Scale. J Atmos Sci 63:2548–2566. https://doi.org/10.1175/JAS3753.1

Haynes P, Scinocca J, Greenslade M (2001) Formation and maintenance of the extratropical tropopause by baroclinic eddies. Geophys Res Lett 28(22):4179–4182. https://doi.org/10.1029/2001GL013485

Held IM (1982) On the height of the tropopause and the static stability of the troposphere. J Atmos Sci 39:412–417. https://doi.org/10.1175/1520-0469(1982)039%3c0412:OTHOTT%3e2.0CO;2

Highwood EJ, Hoskins BJ, Berrisford P (2000) Properties of the Arctic tropopause. Q J R Meteorol Soc 126:1515–1532

Hitchcock P, Simpson IR (2014) The downward influence of stratospheric sudden warmings. J Atmos Sci 71:3856–3876. https://doi.org/10.1175/JAS-D-14-0012.1

Holton JR (2004) An introduction to dynamics meteorology. Academic Press, New York

Huang J, Tian W, Zhang J, Huang Q, Tian H, Luo J (2017) The connection between extreme stratospheric polar vortex events and tropospheric blockings. Q J R Meteorol Soc 143:1148–1164. https://doi.org/10.1002/qj.3001

Jucker M (2016) Are sudden stratospheric warmings generic? Insights from an idealized GCM. J Atmos Sci 73:5061–5080. https://doi.org/10.1175/JAS-D-15-0353.1

Kidston J, Scaife AA, Hardiman SC, Mitchell DM, Butchart N, Baldwin MP, Gray LJ (2015) Stratospheric influence on tropospheric jet streams, storm tracks and surface weather. Nat Geosci 8:433–440. https://doi.org/10.1038/NGEO2424

Kim KY, North GR (1997) EOFs of harmonizable cyclostationary processes. J Atmos Sci 54:2416–2427

Kim KY, North GR, Huang J (1996) EOFs of one-dimensional cyclostationary time series: computations, examples, and stochastic modeling. J Atmos 53:1007–1017

Kim KY, Hamlington BD, Na H (2015) Theoretical foundation of cyclostationary EOF analysis for geophysical and climatic variables: concepts and examples. Earth Sci Rev 150:201–218

Limpasuvan V, Hartmann DL (2000) Wave-maintained annular modes of climate variability. J Clim 13(24):4414–4429. https://doi.org/10.1175/1520-0442(2000)013%3c4414:WMAMOC%3e2.0.CO;2

Limpasuvan V, Thompson DWJ, Hartmann DL (2004) The life cycle of the Northern Hemisphere sudden stratosphere warmings. J Clim 17:2584–2596

Limpasuvan V, Hartmann DL, Thompson DWJ, Jeev K, Yung YL (2005) Stratosphere-troposphere evolution during polar vortex intensification. J Geopys Res Atmos 110:D24101. https://doi.org/10.1029/2005JD006302

Lorenz DJ, DeWeaver ET (2007) Tropopause height and zonal wind response to global warming in the IPCC scenario integrations. J Geophys Res Atmos 112:D10119. https://doi.org/10.1029/2006JD008087

Martineau P, Son SW (2010) Quality of reanalysis data during stratospheric vortex weakening and intensification events. Geophys Res Lett 37:L22801. https://doi.org/10.1029/2010GL045237

Maycock AC, Hitchcock P (2015) Do split and displacement sudden stratospheric warmings have different annular mode signatures? Geophys Res Lett 42(24):10943–10951. https://doi.org/10.1002/2015GL066754

Mitchell DM, Gray LJ, Anstey J, Baldwin MP, Charlton-Perez AJ (2013) The influence of stratospheric vortex displacements and splits on surface climate. J Clim 26(8):2668–2682. https://doi.org/10.1175/JDLI-D-12-00030.1

Polvani LM, Waugh DW (2004) Upward wave activity flux as a precursor to extreme stratospheric events and subsequent anomalous surface weather regimes. J Clim 17:3548–3554. https://doi.org/10.1175/1520-0442(2004)017%3c3548:UWAFAA%3e2.0.CO;2

Rieckh T, Scherllin-Pirscher B, Ladstädter F, Foelsche U (2014) Characteristics of tropopause parameters as observed with GPS radio occulation. Atmos Meas Tech 7:3947–3958. https://doi.org/10.5194/amt-7-3947-2014

Runde T, Dameris M, Garny H, Kinnison DE (2016) Classification of stratospheric extreme events according to their downward propagation to the troposphere. Geophys Res Lett 43:6665–6672. https://doi.org/10.1002/2016GL069569

Seidel D, Randel W (2006) Variability and trends in the global tropopause estimated from radiosonde data. J Geophys Res 111:D21101. https://doi.org/10.1029/2006JD007363

Seviour WJM, Gray LJ, Mitchell DM (2016) Stratospheric polar vortex splits and displacements in the high-top CMIP5 climate models. J Geophys Res Atmos 121:1400–1413. https://doi.org/10.1002/2015JD024178

Simpson IR, Blackburn M, Haigh JD (2009) The role of eddies in driving the tropospheric response to stratospheric heating perturbations. J Atmos Sci 66:1347–1365. https://doi.org/10.1175/2008JAS2758.1

Thompson DW, Wallace JM (1998) The Arctic Oscillation signature in the wintertime geopotential height and temperature fields. Geophys Res Lett 25:1297–1300

Thompson DW, Wallace JM (2000) Annular modes in the extratropical circulation part I: month-to-month variability. J Clim 13:1000–1016. https://doi.org/10.1175/1520-0442(2000)013%3c1000:AMITEC%3e2.0.CO;2

Tomassini L, Gerber EP, Baldwin MP, Bunzel F, Giorgetta M (2012) The role of stratosphere-troposphere coupling in the occurrence of extreme winter cold spells over northern Europe. J Adv Model Earth Syst 4:M00A03. https://doi.org/10.1029/2012MS000177

Vallis GK (2006) Atmospheric and oceanic fluid dynamics: fundamentals and large-scale circulation. Cambridge University Press, Cambridge, pp 522–258

Wang R, Tomikawa Y, Nakamura T, Huang K, Zhang S, Zhang Y, Yang H, Hu H (2016) A mechanism to explain the variations of tropopause and tropopause inversion layer in the Arctic region during a sudden stratospheric warming in 2009. J Geophys Res Atmos 121:11932–11945. https://doi.org/10.1002/2016JD024958

Wong S, Wang W-C (2000) Interhemispheric asymmetry in the seasonal variation of the zonal mean tropopause. J Geophys Res Atmos 105:26645–26659. https://doi.org/10.1029/2000JD900475

Wong S, Wang W-C (2003) Tropical-extratropical connection in interannual variation of the tropopause: comparison between NCEP/NCAR reanalysis and an atmospheric general circulation model simulation. J Geophys Res Atmos 108(D2):4043. https://doi.org/10.1029/2001JD002016

World Meteorological Organization (WMO) (1957) Meteorology a three-dimensional science: second session of the commission for aerology. WMO Bull 4:134–138

Zängl G (2002) Dynamical heating in the polar lower stratosphere and its impact on the tropopause. J Geophys Res Atmos 107:4079. https://doi.org/10.1029/2001JD000662

Zängl G, Hoinka KP (2001) The tropopause in the polar regions. J Clim 14:3117–3139

Zängl G, Wirth G (2002) Synoptic-scale variability of the polar and subpolar tropopause: data analysis and idealized PV inversions. Q J R Meteorol Soc 128:2301–2315. https://doi.org/10.1256/qj.01.76

Zhang K, Wang T, Xu M, Zhang J (2019) Influence of wintertime polar vortex variation on the climate over the North Pacific during late winter and spring. Atmosphere 10(670):1–17. https://doi.org/10.3390/atmos10110670